Applied Surface Science 509 (2020) 145358

Contents lists available at ScienceDirect

Applied Surface Science

journal homepage: www.elsevier.com/locate/apsusc

Full Length Article

Assembling ZnO and Fe_3O_4 nanostructures on halloysite nanotubes for anti-bacterial assessments

Seung-Cheol Jee[a], Min Kim[a], Surendra K. Shinde[b], Gajanan S. Ghodake[b], Jung-Suk Sung[a], Avinash A. Kadam[c,*]

[a] Department of Life Science, College of Life Science and Biotechnology, Dongguk University-Seoul, Biomedi Campus, 32 Dongguk-ro, Ilsandong-gu, Goyang-si 10326, Gyeonggi-do, South Korea
[b] Department of Biological and Environmental Science, College of Life Science and Biotechnology, Dongguk University-Seoul, 32, Dongguk-ro, Ilsandong-gu, Goyang-si, Gyeonggi-do 10326, South Korea
[c] Research Institute of Biotechnology and Medical Converged Science, Dongguk University-Seoul, Biomedi Campus, 32 Dongguk-ro, Ilsandong-gu, Goyang-si 10326, Gyeonggi-do, South Korea

ARTICLE INFO

Keywords:
Halloysite nanotubes
Nano-anti-microbials
MRSA
E. coli
S. *aureus*
Biofilms

ABSTRACT

This study reports anti-bacterial assessments of 'halloysite nanotubes (HNTs) surface-tuned with Fe_3O_4 and ZnO nanostructures (M-HNTs-ZnO)' against the non-drug resistant pathogenic *E. coli* and *S. aureus*, drug-resistant methicillin-resistant *S. aureus* (MRSA) and their respective biofilms. Naturally occurring clay mineral the halloysite nanotubes (HNTs) are emerging materials in nano-bio-medicines. Fabricating HNTs' tunable surface with anti-bacterial nanomaterials can be a significant application in combating the deadly bacterial infections. SEM, TEM, FT-IR, XPS and VSM analysis corroborated a successful synthesis of M-HNTs-ZnO. The acquired results established the significant anti-bacterial potential of M-HNTs-ZnO against the *E. coli*, *S. aureus* and MRSA, respectively. The stepwise modifications made on HNTs enhanced anti-bacterial performance. Detailed SEM image analysis established possible anti-bacterial mechanisms. M-HNTs-ZnO found effective against the successfully established biofilms of *S. aureus*. The M-HNTs-ZnO applied in repeated anti-bacterial performance against *E. coli*, *S. aureus* and MRSA, marked its importance for water-treatments. In conclusion, M-HNTs-ZnO showed significant anti-bacterial properties that can be used in the treatment of infectious diseases. Also, its repeated anti-bacterial capabilities might be applied in water disinfection protocols.

1. Introduction

The use of antibiotics dominated as a treatment for the pathogenic micro-organisms in the last century [1]. The dramatic increase in antibiotic resistance of pathogenic bacteria constitutes one of the major threats to human health [1,2]. To combat these problems, several antimicrobial nanomaterials have been studied in recent years for the replacement of antibiotics. Despite this, the robust nano-material with natural-availability, higher-efficiency, and multi-functional properties are necessary to be investigated. However, the highly-applicable and multi-dimensional materials which have the anti-bacterial effect to methicillin-resistant *Staphylococcus aureus* (MRSA) and their biofilms can counter the rising drug-resistance in micro-organisms.

Halloysite nanotubes (HNTs) are the biocompatible materials, known for exceptional drug carrier potential [3-6]. HNTs are naturally occurring clay mineral having a significant potential of the surface modification for diverse applications [3]. Structurally, HNTs $[Al_2Si_2O_5(OH)_4{\cdot}2H_2O]$ are made up of aluminosilicate layers with the composition of aluminum, silicon, hydrogen, and oxygen [7]. HNTs structure shows hollow-tubular nature with an inner-lumen diameter of 5–20 nm and the length of the tube is in the range of 0.5–10 μm [8]. Chemistry of HNTs includes a tubular morphology with the Al—OH sheet forming the inside and the Si–O sheet the outside [9,10]. The HNTs' outer surface mainly covered by Si—O—Si groups and have some Si—OH groups present on the edges [11]. HNTs nano-tubular framework provides there utilization in diverse applications including; environmental, catalytic, and nano-medicinal [12]. Due to their outstanding properties, HNTs are widely used in many emerging applications. So, the impact of the HNTs on human health and the environment needs to test. The biocompatibility of HNT is one of the

* Corresponding author. Research Institute of Biotechnology and Medical Converged Science, Dongguk University-Seoul, Biomedi Campus, 32 Dongguk-ro, Ilsandong-gu, Goyang-si 10326, Gyeonggi-do, South Korea.
E-mail addresses: avikadam2010@gmail.com, kadamavinash@dongguk.edu (A.A. Kadam).

https://doi.org/10.1016/j.apsusc.2020.145358
Received 4 September 2019; Received in revised form 30 December 2019; Accepted 10 January 2020
Available online 12 January 2020
0169-4332/

main necessities for use in personal care products [13]. Recent reports of *in vitro* and *in vivo* toxicity evaluations of HNTs revealed HNTs biocompatible nature [13-16]. When HNTs were modified with iron oxide (Fe_3O_4) nanoparticles, HNTs reduced the cytotoxicity of Fe_3O_4 nanoparticles by changing their surface characteristics [13,17]. Based on the several animal modal studies, HNTs clay is the safest biocompatible material and is much less harmful than the carbon nanomaterials such as carbon nanotubes [16].

HNTs loaded with nanomaterials/anti-microbial compounds have been utilized for anti-microbial activities [5,18-24]. Therefore, decorating the HNTs surface with applied nanomaterials aids significant applications in nanomedicines [12]. The unique structural properties of HNTs laid a solid platform, to develop further exceptional materials. Iron oxide nanoparticles (Fe_3O_4) are highly known for their rapid-separation from the solution due to the magnetic potential [25]. The use of Fe_3O_4 nanoparticles separation-potential in anti-microbial treatment of water and waste-waters was significantly important to combat pathogenic bacteria [25]. Inorganic antimicrobials zinc oxide (ZnO) nanoparticles known for properties such as; better selectivity, lower cytotoxicity, heat resistance and higher stability [26]. Remarkably, ZnO nanoparticles are reported as non-toxic to human cells [27]. Therefore, assembling these nanomaterials (Fe_3O_4 and ZnO) over HNTs can give magnetic anti-microbial nano-tubular reactors, which might be accessed for the anti-bacterial potential against non-drug resistant and drug-resistant pathogenic bacteria's, and their biofilms. In addition to this, the Fe_3O_4 and ZnO also possess a wide range of applications like; separation-science, environmental remediation of pollutants and the solar cells etc [4,7,8,28-34]. However, this study mainly aimed to evaluate Fe_3O_4 and ZnO modified HNTs against the 'non-drug resistant pathogenic bacteria's, drug-resistant MRSA, biofilm infections and repeated anti-bacterial effect in many cycles'.

In summary, this study aimed to fabricate HNTs based nano-anti-microbial material, by assembling Fe_3O_4 (M-HNTs) and ZnO (M-HNTs-ZnO) nanoparticles on the HNTs tunable surface. The developed nano-anti-microbial materials tested against individual non-drug resistant pathogenic-bacteria such as; *E. coli* and *S. aureus*, drug-resistant MRSA strain, and their efficacy to treat biofilms (biofilms of *E. coli*, *S. aureus*, and *MRSA*). Also, the repeated use of M-HNTs-ZnO for the anti-bacterial response was investigated. Thus, this overall strategy targeted a complete anti-bacterial evaluation of developed HNTs based nano-anti-microbial material.

2. Materials and methods

2.1. Materials and microbial strains

HNTs, Na_2SO_3 and NaOH were obtained from Sigma Aldrich, USA. Zinc acetate and iron(III) chloride hexahydrate were obtained from the Dae Jung Chemicals, South Korea. *Escherichia coli* (KCCM 11234; *E. coli*), *staphylococcus aureus* (KCCM 11335; *S. aureus*), and methicillin-resistant *staphylococcus aureus* (ATCC 33591; MRSA) were obtained from the Korean Culture Center of Microorganisms (KCCM, Seoul, Korea) and the American Type Culture Collection (ATCC, VA, USA). Each bacterium was cultured on a Tryptic Soy Agar plate (TSA; BD, San Jose, CA, USA). The TSA plates were incubated at 37 °C for overnight. Each colony of the bacterium was inoculated in Tryptic Soy Broth (TSB; BD, San Jose, CA, USA) and incubated at 37 °C 150 rpm for 18 h.

2.2. Synthesis

HNTs were super-magnetized by the reduction-precipitation method [4]. In a typical reduction-precipitation method, 1 gm of HNTs was added in 100 mL distilled water. The mixture was refluxed and ultrasonicated for 1 h. Then 50 mL of $FeCl_3.6H_20$ solution (3%) was added dropwise. The reductant solution of Na_2SO_3 (0.7%) was added to the mixture. After the addition of the Na_2SO_3, the color of the solution was changed to the wine red and further back to the yellow within 2 min of time. Once the color changed to the yellow color, the precipitant 30 mL solution of NaOH (1 M) was added. This formed a dark black colored precipitate. The precipitate was refluxed for 10 min and separated by an external magnetic field applied. The separated magnetized HNTs (M-HNTs) was used further in the experiment. Further, M-HNTs were modified with the zinc oxide nanoparticles as reported by [32], with several modifications. In a typical synthesis process, M-HNTs (0.5 g) was taken in 20 mL separately in 100 mL beaker. The respective solutions were mixed thoroughly and ultrasonicated for 20 min. After mixing and ultrasonication process, 20 mL of $ZnAc_2{\cdot}2H_2O$ solution (5%) was added dropwise to M-HNTs mixtures. These mixtures were rapidly refluxed for 12 h on the magnetic stirrer. The precipitates formed in both the mixtures were washed several times with distilled water and solid pellet were dried at vacuum oven (65 °C) for 24 h. The dried powders were calcinated at 500 °C for 3 h. The obtained dry powders of M-HNTs-ZnO were dried and ground for further use.

2.3. Characterizations

Functional-groups of the materials were analyzed by Fourier transform infrared spectroscopy (FT-IR, Vertex 80v (Bruker) Germany), using the KBr pellet method (KBr ~ 0.15 g and sample < 0.001 g). The nanoparticulate nature and surface morphology of materials were witnessed by scanning electron microscopy (SEM, FC-SM10, Hitachi S-4800, Japan) and transmission electron microscopy (TEM, Tecnai G2, Hillsboro, USA). The surface elemental composition of the materials was examined by X-ray photoelectron spectroscopy (XPS, Theta Probe AR-XPS System, Thermo Fisher Scientific, UK). Magnetic properties of Fe_3O_4 modified materials were analyzed by vibrating sample magnetometer (VSM) (Lakeshore, Model: 7407, USA).

2.4. Anti-bacteria assays

The antibacterial effect of HNTs, M-HNTs, and M-HNTs-ZnO was estimated against *E. coli* and *S. aureus*, and MRSA. The samples of HNTs, M-HNTs, and M-HNTs-ZnO ultrasonicated for 15 min before the use. Each bacterium having initial concentration of 0.6–1.0 of OD 600 nm prepared in the trypticase soy broth (TSB) medium. The HNTs, M-HNTs, and M-HNTs-ZnO at the concentration of 5 mg/ml were added into the medium and incubated at 37 °C for 4 h with 1×10^6 cells/ml bacteria 180 rpm in the shaking condition. After incubation, anti-bacteria effects were evaluated using colony counting assay on agar plate and petrifilm (3 M, MN, USA). Inoculated bacteria were seeded on both trypticase soy agar and petrifilm incubated at 37 °C for 24 h, and then photographs of anti-bacteria effects.

2.5. Anti-biofilm assay

Formation of bacterial biofilms of *E. coli* and *S. aureus* and MRSA for studying the anti-biofilm effect was referred by [35]. Inhibition effect of HNTs, M−HNTs, and M-HNTs-ZnO against biofilm formation was estimated on a 6-well plate using Crystal violet (CV) assay. Each bacterial strain was cultured in TSB and dispensed into 6-well plate. Seeded bacteria were incubated at 37 °C for 24 h. The 24 grown bacterial culture in a 6-well plate was washed two times with the PBS. HNTs and modified HNTs at the concentration of 5 mg/ml were added in 6-well plate 24 grown bacterial cultures and incubated at 37 °C for 4 h. After then, the well was washed two times with PBS and 0.1% CV solution was added to each well for 5 min. After taken a picture, added to 33% acetic acid each well and estimated to absorbance at 590 nm.

2.6. Scanning electron microscopy (SEM) analysis

E.coli, S. aureus, and MRSA were incubated with HNTs, M-HNTs, and M-HNTs-ZnO at 37 °C under 150 rpm shaking speed for 4 h. All

cells were collected and rinsed twice with phosphate-buffered saline (PBS, Bio-sesang, Seoul, Korea), followed by fixing with a 2.5% glutaraldehyde solution at 4 ˚C for 18 h. The samples were dehydrated by treatment with 50, 70, 80, 90 and 100% ethanol respectively. Each sample was coated with a thin layer of gold and imaged via SEM.

2.7. Repeated cycle antibacterial effect by M-HNTs-ZnO

The anti-bacterial effect of M-HNTs-ZnO was measured against *E. coli* and *S. aureus*, and MRSA. Each 24 h grown bacterium was incubated at 37 ˚C for 4 h with M-HNTs-ZnO at 180 rpm in the shaking condition and evaluated for the bacterial viability. After incubation, microbial viability was measured using microbial viability assay ELISA kit (Dojindo, Kumamoto, Japan) according to the manufacturer's instructions. After then, M-HNTs-ZnO was separated using an external magnet and sterilized using autoclave 121 ˚C for 15 min. Sterilization was done to overcome the problem arising from the attached bacteria's to the M-HNTs-ZnO. Sterilized M-HNTs-ZnO was further applied in the next cycle to study the repeated anti-bacterial effect.

3. Results and discussions

3.1. Synthesis

In recent literature, HNTs found to be excellent material in many nano-medicinal and environmental applications [3]. Although, there are many aspects of HNTs applications, which still needs to be studied and investigated [3]. Hence, in this study, surface modifications on the HNTs were done by incorporating the Fe_3O_4 and ZnO nanostructures. The detailed schematic presentation was shown in Scheme 1. First, Fe_3O_4 was decorated over the HNTs (M-HNTs) by a low-cost reduction-precipitation (RP) method. Later, ZnO nanoparticles were assembled over the M-HNTs. The Zn^{2+} ions from precursor solution of zinc acetate binds tightly over the negative surface of the HNTs and nucleation of Zn^{2+} ions occurred after calcination at 500 ˚C, to form the ZnO over M-HNTs surface. Because of the HNTs as a template for the distribution of ZnO, aggregation of ZnO was inhibited. Therefore, these nanotubular reactors possess the magnetism from Fe_3O_4 (allows their systematic localization and separation) and significant anti-microbial potential from the ZnO nanostructures. The materials; HNTs, M-HNTs, and M-HNTs-Zn was assessed further in the study for anti-microbial, anti-MRSA and anti-biofilm studies.

3.2. Characterization's

3.2.1. SEM and TEM analyses

The morphological observation was done by the SEM analysis. The SEM image of HNTs, M-HNTs, and M-HNTs-Zn was shown in Fig. 1A–C. The image of HNTs showed random nanotubes with the unmodified surface (Fig. 1A). The M-HNTs SEM image showed a Fe_3O_4 modification of HNTs (Fig. 1B). However, in the M-HNTs-ZnO sample, extensive surface modification was clearly evident (Fig. 1C). Circular and square-shaped morphologies of ZnO nanostructures seen to be decorated an HNTs surface (Fig. 1C). In order to investigate morphological observations, further TEM analysis was done. Fig. 1D shows the image of the HNTs, and the surface of the HNTs looks plane and unmodified. However, the TEM image of the M-HNTs-ZnO (Fig. 1E), clearly showed an extensively modified surface of various sized HNTs with the Fe_3O_4 and ZnO nanostructures. Cuboidal and square-shaped ZnO nanostructures evident on the HNTs surface and seen bind tightly to HNTs. Further, more close inspection of ZnO nanostructures in a zoomed image (Fig. 1F) revealed a size of around 5–6 nm. The lattice fringe region of 0.25 nm corroborates (0 0 2) crystalline plane of the ZnO. Therefore, all these morphological analyses confirmed the surface of the HNTs was modified by a Fe_3O_4 and ZnO nanostructures.

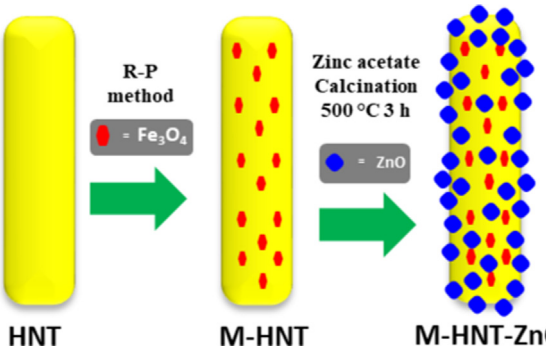

Scheme 1. Schematic presentation of stepwise synthesis of M-HNT-ZnO.

3.2.2. FT-IR and VSM analysis

In order to investigate the successful modifications made on HNTs, the FT-IR spectrums were analyzed. Fig. 2(A) shows the FT-IR spectrum of the HNTs, M − HNTs, and M-HNTs-ZnO. The FT-IR spectrum of HNTs and M-HNTs gave the following absorption peaks at 3695 cm^{-1} (the inner surface O—H stretching of HNTs), 3621 cm^{-1} (O—H stretching of inner surface Al—OH groups between the interface of the Si—O tetrahedron and the Al—O octahedron), 1031 cm^{-1} (in-plane stretching vibration of the Si—O network Si—O—Si and O—Si—O) and 911 cm^{-1} (O—H deformation of inner hydroxyl groups) [36].

The FT-IR peak for Al—O—Si of HNTs and the characteristic peak of metal oxides (Fe-O and Zn—O) might be overlapped in a spectrum of HNTs, M-HNTs and M-HNTs-ZnO [4,8,37]. However, the M-HNTs-ZnO exhibits broad absorption peaks observed at 3441 cm^{-1} was attributed to the O—H groups on the surface of the ZnO [37]. Similar at 3441 cm^{-1} peak broadening in ZnO-PEG nano-hybrids was observed previously [37]. The obtained results are consistent with the observation made in the SEM and TEM image analysis. The incorporation of Fe_3O_4 gave magnetic properties to the M-HNTs-ZnO. Therefore, it was important to study magnetic properties. The magnetic properties of M-HNTs-ZnO were studied by VSM analyses (Fig. 2(B)). In order to understand the magnetic properties of M-HNTs-ZnO, the VSM analysis was carried out. The curve obtained from the VSM analysis of M-HNTs-ZnO demonstrates a typical magnetic hysteresis (Fig. 2(B)). The obtained values of the coercivity and remanence were zero. Thus, the typical magnetic hysteresis curve and obtained zero values of coercivity and remanence were confirmed the superparamagnetic nature of the M-HNTs-ZnO [38]. The magnetization saturation value represents the susceptibility of a sample to an external magnetic field. The magnetic saturation value of the M-HNTs-ZnO was found to be 3.8 emu/g. The inset of Fig. 2(B) showed the magnetic separation potential of the M-HNTs-ZnO. Therefore, FTIR analyzes gave an idea about the HNTs modification by Fe_3O_4 and ZnO, respectively, and VSM analysis confirmed the magnetic potential of M-HNTs-ZnO.

3.2.3. XPS analysis

Furthermore, validation of the M-HNTs-ZnO material was done by XPS analysis. The XPS of M-HNTs-ZnO was shown in Fig. 3. The observed binding energies 74.65, 102.58, 532.4, 711.13 and 1022.2 eV attributed to the Al 2p, Si 2p, O 1 s, Fe 2p, and Zn 2p, respectively (Fig. 3a). Thus, the obtained results strongly corroborate the successful synthesis of nanocomposite M-HNTs-ZnO. The obtained XPS results validated the SEM, TEM, and FT-IR analyzes studied. Furthermore, higher resolution spectrums of Si 2p, O 1s, Al 2p, Fe 2p, and Zn 2p were shown in Fig. 3b–f. The high resolutions spectrums show a clear and sharp peak of the respective element (Si, O, Al, Fe, and Zn). The high-resolution spectra of Fe 2p (Fig. 3e) show the characteristic Fe_3O_4 peaks of Fe $2p_{1/2}$ and Fe $2p_{3/2}$ located at 711.48 and 725.23 eV respectively. The peaks are broadened due to the existence of the Fe^{2+} and Fe^{3+} ions as Fe_3O_4. A similar observation for Fe_3O_4/rGO nanocomposites was

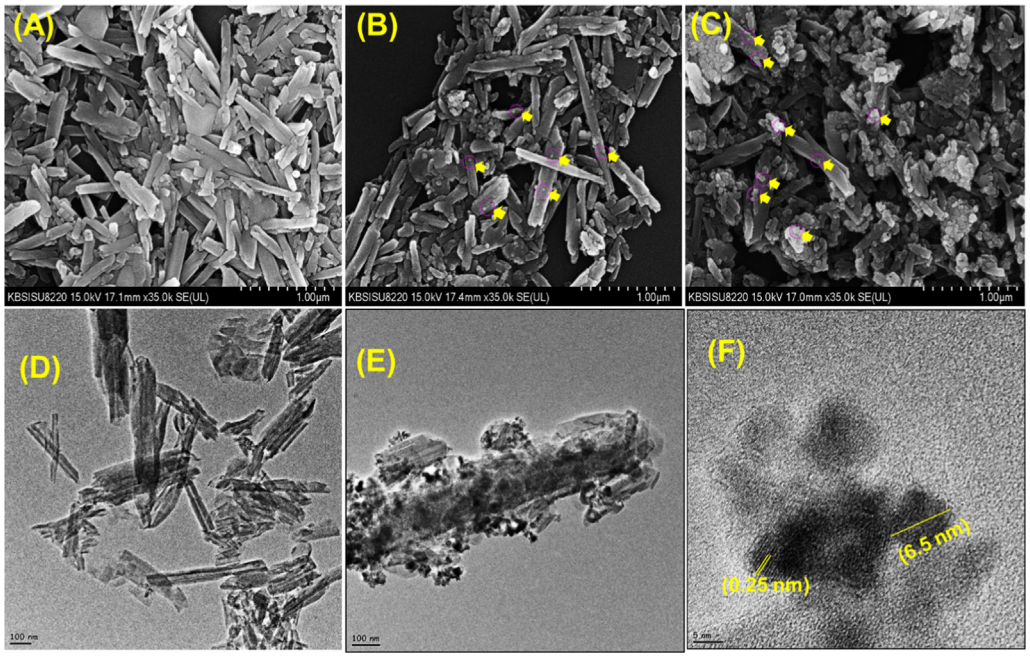

Fig. 1. Surface morphological evaluation [A] SEM image of HNTs, [B] SEM image of M-HNTs, [C] SEM image of M-HNTs-ZnO, [D] TEM image of HNTs, [E] TEM image of M-HNTs-ZnO and [F] high resolution of TEM image displaying the lattice fringe regions and particular size of ZnO loaded over the HNTs.

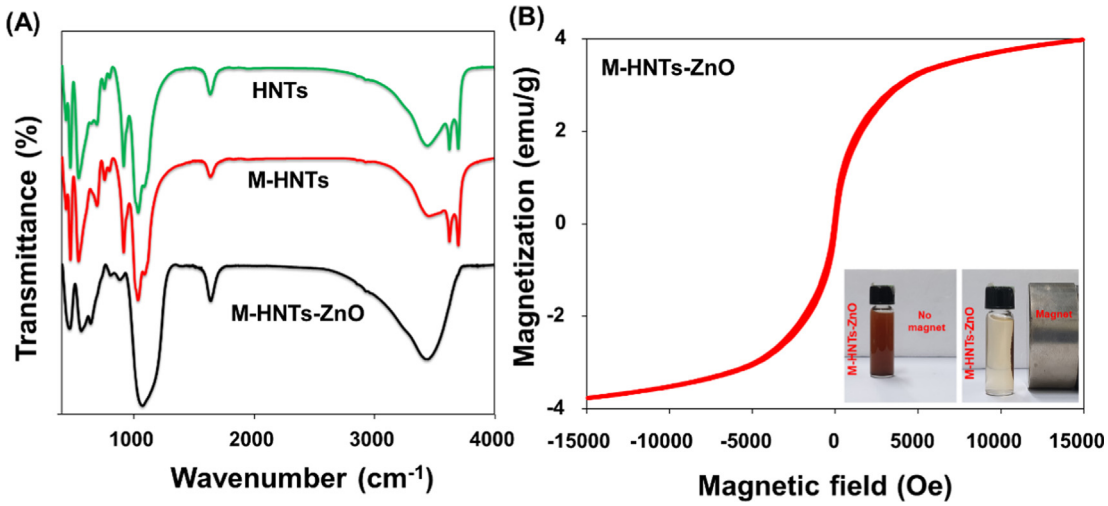

Fig. 2. (A) FTIR analysis of HNTs, M-HNTs, and M-HNTs-ZnO, and (B) VSM analysis of M-HNTs-ZnO and the photographic image showing magnetization.

reported earlier [39]. The high-resolution spectra of Zn 2p (Fig. 3f) exhibited binding energies of 1022.15 and 1045.25 eV, attributed to the spin-orbit of Zn $2p_{3/2}$and Zn $2p_{1/2}$. It directed the presence of a divalent oxidation state in the sample [40].

Therefore, the entire XPS evaluation confirmed the M-HNTs-ZnO composed of HNTs (Si, Al, and O), Fe_3O_4 (Fe) and ZnO (Zn). Thus, the entire characterization's; SEM, TEM, FTIR, VSM, and XPS analyses validated the successful synthesis. The materials after thorough characterization were used in further study.

3.3. Anti-bacterial studies against E. Coli and S. Aureus

The HNTs, M-HNTs, and M-HNTs-ZnO were applied to study anti-bacterial effect to the *E. coli* (Gram-negative) and *S. aureus* (Gram-positive). These are the typical bacteria that are most often found in infections, contaminated equipment, and wounds. The anti-bacterial effects of HNTs, M-HNTs, and M-HNTs-ZnO (5 mg/ml) were confirmed using the colony counting assay. The results were shown in Fig. 4A-B. HNTs showed significant anti-bacterial potential (62% growth inhibition of *E. coli*). The obtained result supported by the earlier report, which showed a slight decrease in the number of *E. coli* cells in the presence of the bare HNTs [5]. Also, Taylor et al., [41] report the reduction in the growth of *S. typhimurium oxyR* strain in the presence of HNTs. In this study, during the anti-bacterial experiment 'HNTs with bacterial cells' was shaken at 180 rpm speed and this might cause an enhancement of physical damage/rupture to the bacterial cells. The increased interactions among the HNTs and bacterial cells at 180 rpm speed might be yielded the anti-bacterial potential of HNTs. Anti-bacterial HNTs are highly valuable, as it is a naturally derived material. This obtained result encouraged to advance/modify the HNTs surface by various anti-microbial nanomaterials. Because of Fe_3O_4 NPs exclusive characteristics, such as response to external magnetic force (magnetic assistance) is extremely important in case of the critical localization of infection [42,43]. The Fe_3O_4 nanomaterial is a metal oxide that possesses both anti-bacterial and magnetic properties [17]. Different studies reported the anti-microbial potential of Fe_3O_4 is might be

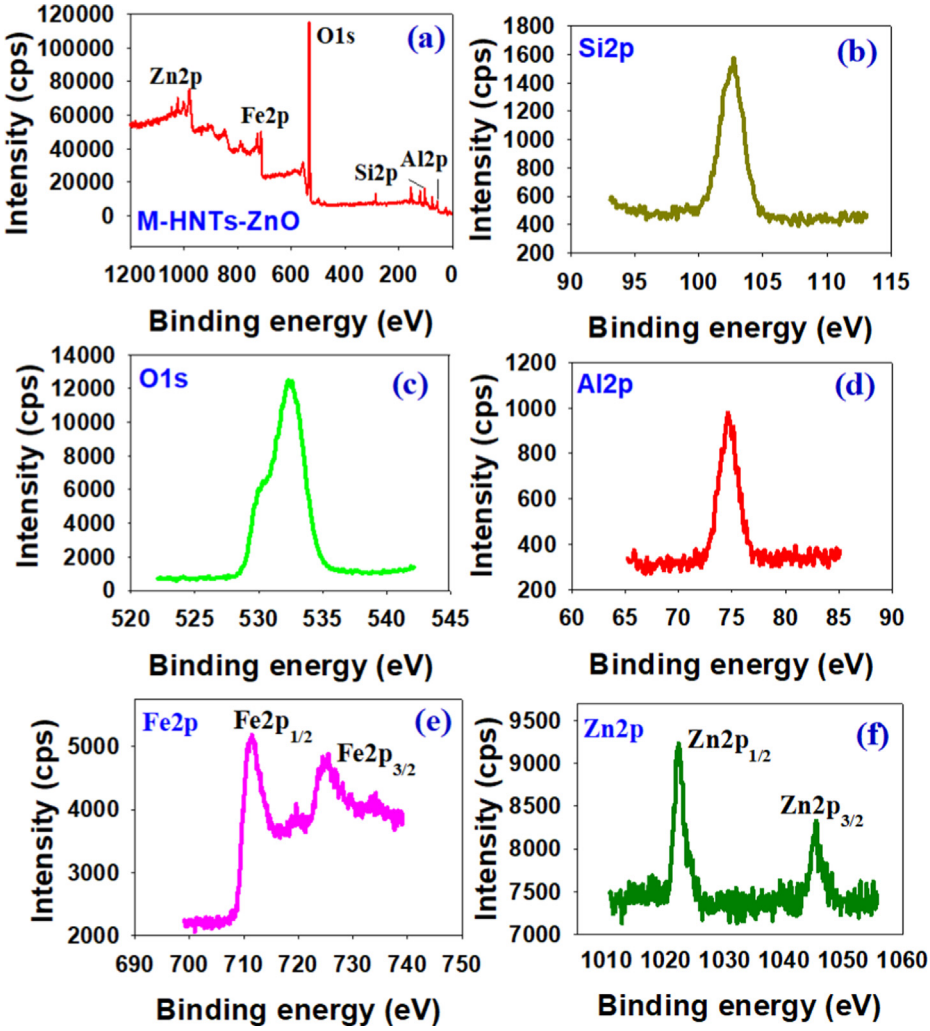

Fig. 3. XPS analysis of (a) Survey spectrum of M-HNTs-ZnO, high resolution spectrum of (b) Si2p, (c) O1s, (d) Al2p, (e) Fe2p and (f).

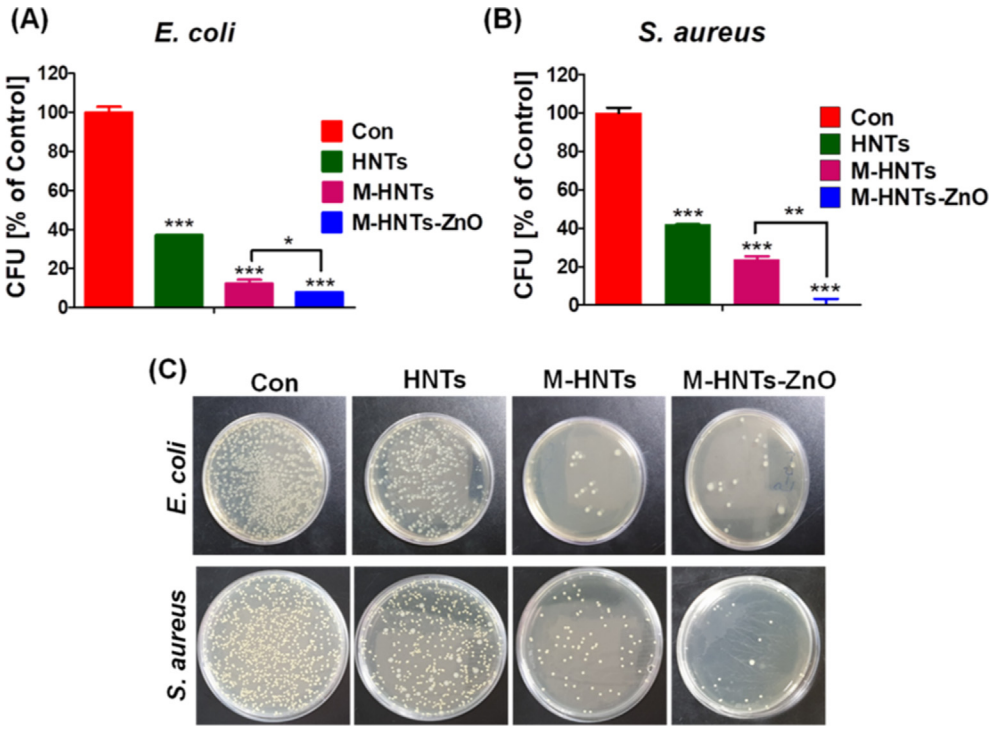

Fig. 4. Anti-bacteria effect of HNTs, M-HNTs, and M-HNTs-ZnO against (A) *E. coli* and (B) *S. aureus*. All values are expressed as mean ± SEM (n = 3) and significantly different (*, $p < 0.05$, **, $p < 0.01$, ***, $p < 0.005$) in comparison to control by Tukey's multiple comparison test. (C) Photographs of bacteria colonies formed treated with HNTs, M-HNTs, and M-HNTs-ZnO against *E. coli* and *S. aureus*.

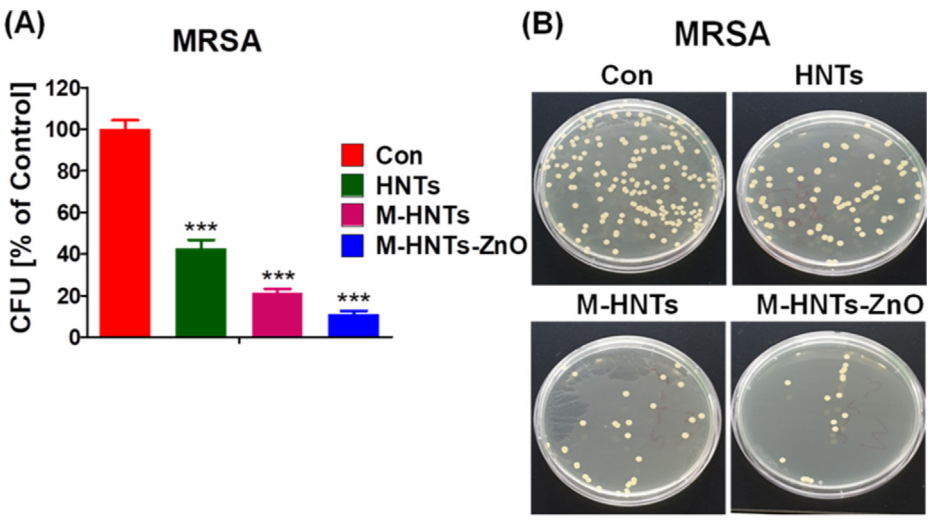

Fig. 5. (A) Anti-bacteria effect of HNTs, M-HNTs, and M-HNTs-ZnO against MRSA. All values are expressed as mean ± SEM (n = 3) and significantly different (*, $p < 0.05$, **, $p < 0.01$, ***, $p < 0.005$) in comparison to control by Tukey's multiple comparison test. (B) Photographs of bacteria colonies formed treated with HNTs, M-HNTs, and M-HNTs-ZnO against MRSA.

due to the production of reactive oxygen species (ROS) with lipid peroxidation, membrane depolarization with consequent impairment of cell integrity, the release of metal ions that affect cellular homeostasis and protein coordination and DNA damage [17,25]. Abhinaya et al., [17] reported that M-HNTs have antibacterial activity against *E. coli* which less than the anti-bacterial activity of Fe_3O_4 NPs at different phases of the growth. However, in this study, HNTs surface modified by the Fe_3O_4 (M-HNTs) exhibited enhanced anti-bacterial activity (87% growth inhibition of *E. coli*). The anti-bacterial activity to *E. coli* by M-HNTs was enhanced compared to the HNTs. This increase in growth inhibition of *E. coli* was due to the enhanced anti-bacterial effect exerted by the Fe_3O_4. Furthermore, M-HNTs were modified by ZnO (M-HNTs-ZnO) gave 92.2% of the growth inhibition to *E. coli*. ZnO is a well-known anti-microbial metal oxide nanomaterial and exerts an anti-bacterial effect in several ways such as; generation of reactive oxygen species (ROS), cell wall damage due to ZnO-localized interaction, internalization of ZnO NPs due to loss of proton motive force, enhanced membrane permeability, and toxic zinc ions uptake [27]. Thus, surface modifications of HNTs with (Fe_3O_4 and ZnO) significantly enhanced the anti-bacterial potential against the *E. coli* (Fig. 4A). Furthermore, against the bacteria *S. aureus,* HNTs, M-HNTs and M-HNTs-ZnO inhibited the growth to 58, 76 and 99%, respectively. Similar to the *E. coli*, in the case of anti-bacterial effect to the *S. aureus*, inhibition was enhanced for M-HNTs-ZnO (99%) compared to the M-HNTs (76%) (Fig. 4B). The photographic image of the *E. coli* and *S. aureus* colonies obtained before and after the treatment was confirmed the anti-bacterial potential of the studied materials (Fig. 4C). HNTs modified with CuO NPs, Ag NPs, ZnO NPs, polyurethanes, peppermint essential oil, salicylic acid, thyme oil, and vancomycin were shown anti-bacterial properties [5,6,19-23,25,44-49]. The detailed anti-microbial potentials and studied parameters of HNTs (powder form) based on anti-microbial materials were shown in the supplementary information, Table S1. Silver nanoparticles, Fe_3O_4, silver NPs/ZnO and ZnO/CeO_2 modified HNTs gave approximately 75, 18, 95 and 92% bacterial growth inhibition (supplementary information, Table S1). Hence, in comparison with the earlier HNTs based materials (supplementary information, Table S1), the obtained results suggest the M-HNTs-ZnO is among the highly significant HNTs based antibacterial material.

Notably, the materials exhibited anti-bacterial properties to both Gram-negative and Gram-positive bacteria. The obtained results showed the HNTs, M-HNTs and M-HNTs-ZnO materials are potential antibacterial capabilities and need to further study against the drug-resistant bacteria and bacterial biofilms.

3.4. Anti-bacterial studies against MRSA

When the bacteria carry several resistance genes against more than two antibiotics, it is usually mentioned as multiple-antibiotic-resistant bacteria, superbug or a super-bacterium [50]. Gram-positive drug-resistant bacteria MRSA is a serious threat, and antimicrobial resistance is a major global health concern [51]. MRSA is a dangerous pathogen well known for the resistant against β-lactam antibiotics. In recent times, MRSA was categorized by the World Health Organization (WHO) as one of the twelve priority pathogens that threaten human health [52]. Innovative tactics are consequently desirable to recognize and advance agents to control bacterial infections or the next generation of drugs [50]. Recently, nanotechnology yielded materials that have flourished as an enormously potent and multipurpose nano-weapons to fight these issues [53-55]. Contrary to the mechanistic action of antibiotics, microbes just find problematic to obtain resistance toward nanoparticles as they target multiple bacterial components [50,55]. Zinc oxide (ZnO), iron oxide (Fe_3O_4), titanium dioxide (TiO_2), copper oxide (CuO) and silver nanoparticles (AgNPs) and their composites found bactericidal to the MRSA [1,50]. However, decorating important nanoparticles such as (ZnO and Fe_3O_4) on nanotubular structures of HNTs have a significant impact for MRSA treatment, by considering its biocompatibility and upcoming staggering applications in the nano-medicinal field [[3,4,24]. Therefore, in this study, the anti-bacterial potential of HNTs, M-HNTs, and M-HNTs-ZnO was checked against the MRSA strain (Fig. 5A). The HNTs and M-HNTs showed 57 and 78% growth inhibition of the MRSA (Fig. 5A). M-HNTs showed significantly enhanced MRSA growth inhibition compared to the bare HNTs. In an earlier study, the bare magnetic nanoparticles displayed an anti-microbial effect against the MRSA [56]. Furthermore, MRSA experienced 88% growth inhibition in the vicinity of the M-HNTs-ZnO (Fig. 5A). The photographic image of MRSA colonies before and after the treatment with HNTs, ZnO and Fe_3O_4 NPs has confirmed the inhibition of the growth of MRSA (Fig. 5B).

The obtained results corroborated the stepwise modifications (ZnO and Fe_3O_4) in HNTs increased the anti-bacterial effect on the MRSA. In addition to the HNTs, ZnO and Fe_3O_4 NPs might cause a bacterial death due to their significant anti-microbial potential [6,26,40,50,56]. Being an exceptional and biocompatible drug carrier, HNTs surface modifications with ZnO and Fe_3O_4 gave new hope for the treatment of MRSA [1,24]. Hence, M-HNTs-ZnO has potential anti-bacterial capability against the MRSA, and that might be applicable in the near future.

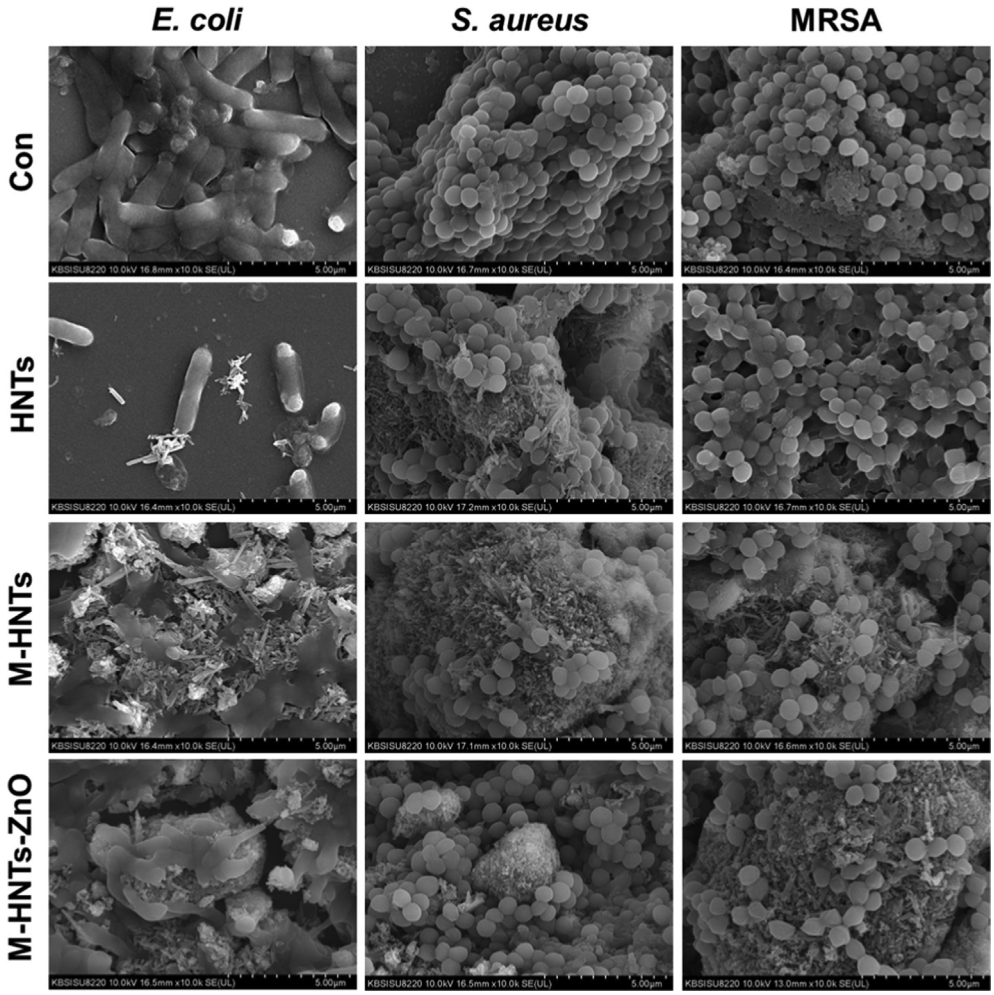

Fig. 6. SEM images of HNTs, M-HNTs, and M-HNTs-ZnO against *E. coli*, *S. aureus*, and MRSA.

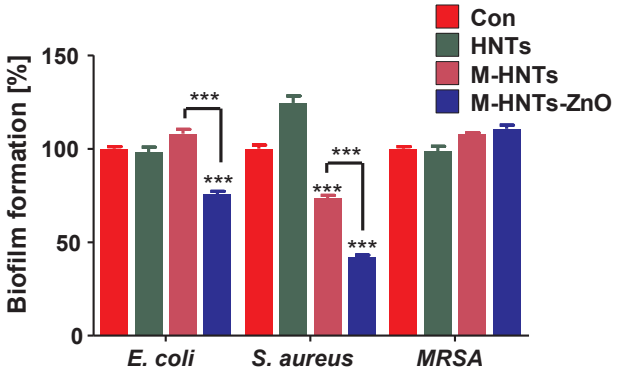

Fig. 7. Anti-biofilm effect of HNTs, M-HNTs, and M-HNTs-ZnO against *E.coli*, *S. aureus*, and MRSA. Each value is expressed as mean ± SEM (n = 3) and significantly different (***, $p < 0.005$) in comparison to control by Tukey's multiple comparison test.

3.5. SEM analysis for bacteria-nanomaterial interactions

After the successful establishment of the anti-bacterial applications of HNTs, M-HNTs, and M-HNTs-ZnO, SEM evaluation was done for understanding the bacteria-nanomaterial interactions. *E. coli*, *S. aureus,* and MRSA strain were observed under SEM before and after the treatment (Fig. 6). The control image shows intact colonies of *E. coli*, *S. aureus,* and MRSA. The images of HNTs shows interaction with *E. coli* caused physical damage, however, not detectable physiological damage was observed with the S. *aureus* and MRSA. This might be due to the differences in the cell wall structures gram-positive and gram-negative. There are few *E. coli* cells, which erupted might be due to the dehydration without the particle contact. However, *S. aureus* and MRSA cells found separated compare to the control. Further, in the case of M-HNTs and M-HNTs-ZnO, *E. coli* showed enhanced interactions and shrinkage of the *E. coli* cells, however, S. *aureus* and MRSA cells have a un-disturbed physical structure with significantly separated cells.

The un-disturbed physical structure attributed to the rigid nature of the gram-positive cell wall. However, the anti-bacterial effect in M-HNTs and M-HNTs-ZnO might be due to the release of the zinc ions, membrane depolarization, generation of the ROS and DNA damage [25,27]. The overall SEM analysis gave bacteria-nanomaterial interactions to understand the obtained anti-bacterial results.

3.6. Anti-biofilm effect of nanomaterials

Looking at the treatment complexity of the biofilm infections of *E. coli*, *S. aureus* and MRSA strain, the HNTs, M-HNTs, and M-HNTs-ZnO were tested for their anti-biofilm effect. The biofilms of *E. coli*, *S. aureus,* and MRSA strain were successfully established. The quantitative analysis of Crystal Violet staining showed in Fig. 7. The obtained results confirmed the HNTs do not exhibit any anti-biofilm effect. The M-HNTs exhibited 25% inhibition of the *S. aureus* biofilm, but not shown inhibition to the *E Coli* and MRSA biofilms. However, M-HNTs-ZnO eliminated the biofilm against *E.coli* (25% inhibition) and *S. aureus*

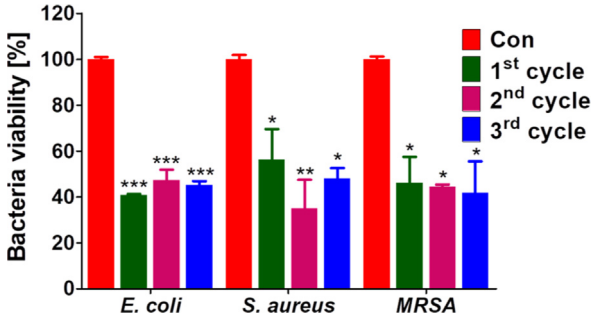

Fig. 8. Anti-bacterial effects of recycled M-HNTs-ZnO against *E. coli*, *S. aureus*, and MRSA. All values are expressed as mean ± SEM (n = 3) and significantly different (*, p < 0.05, **, p < 0.01, ***, p < 0.005) in comparison to control by Tukey's multiple comparison test.

(60% inhibition), but not for MRSA biofilm. The acquired results corroborated the enhanced anti-biofilm activities of M-HNTs-ZnO compared to the HNTs and M-HNTs. This designates the ZnO on HNTs causing a major role in the obtained anti-biofilm effect.

The anti-biofilm effects by nanomaterials are often related to many factors such; as its stability, size, and hydrophobic interaction. Besides, nanomaterials are found induced anti-biofilm effect to different mechanisms such as enzymatic inhibition, deactivation of proteins, and oxidative stress [57]. Anti-biofilm activity of zinc oxide nanosheets (ZnO NSs) against *Proteus mirabilis* and *E.coli* reported by [52]. The exact mechanism of the ZnO mediated anti-biofilm effect was not yet fully understood [58]. Furthermore, MRSA biofilm found resistant to all tested nanomaterials. This might be due to the complex extracellular polymeric substance (EPSs) of MRSA biofilms. These results specify that the anti-biofilm effect of M-HNTs-ZnO was different from *E. coli, S. aureus*, and MRSA biofilms, respectively. Therefore, the anti-biofilm assessments of tested nanomaterials provide glimpses that 'M-HNTs-ZnO' might be a suitable nanomaterial to target the *S. aureus* biofilms particularly.

3.7. Reusability of M-HNTs-ZnO

In this part of the study, the reuse of M-HNTs-ZnO for bactericidal potential was assessed. Drinking water having microbial contamination causes a grave health concern, particularly in developing countries [59]. The most important technique used for domestic water purification is chemical disinfection using chlorine [60]. Chemical disinfectants; chlorine, chloramines, and ozone react with various constituents from natural water and forms a disinfection by-product [59,60]. These disinfection by-products are found to be carcinogens in nature [59]. Recently, nanotechnology opened a new era for water disinfection [61]. Still, two very important challenges that limit the use of nanoparticles for water disinfection are either their aggregation in water or their removal from treated water [62]. To get rid of these difficulties, the nanomaterials combined with a potential magnetic carrier might be a suitable option [62]. Magnetic-separation is controllable, allows the nano-antimicrobial-agents to be recovered effortlessly, ready to reuse for the next cycle of water-purification, and keeping the nano-antimicrobial-agents with reduced environmental-complications. Additionally, the development of clay-based modified materials with high effectiveness to capture bacteria from the water will definitely be advisable due to their ready availability, low-cost and ease of preparation [63]. Therefore, in this study, clay-mineral HNTs based M-HNTs-ZnO having significant magnetic potential was applied for reuse of M-HNTs-ZnO for bactericidal potential against *E. coli* (Gram-negative), *S. aureus* (Gram-positive), and MRSA strain, to access its potential for water treatment (Fig. 8). The obtained results were showed that M-HNTs-ZnO maintained consistent anti-bacteria effects in three cycles compared to the control group against all bacteria studied (Fig. 8).

These results evidenced that M-HNTs-ZnO is easily acquired using magnetic force and apply for the anti-bacteria effects in the next cycle. Thus, this makes M-HNTs-ZnO an economical material having anti-bacterial potential for possible water treatment applications in many cycles.

4. Conclusions

In conclusion, HNTs decorated with anti-microbial and magnetic nanomaterials (Fe_3O_4 and ZnO) displayed significant antibacterial potential against non-drug resistant (*E. coli* and *S. aureus*) and drug-resistant (MRSA) pathogens. The stepwise modification done on template HNTs significantly improved the anti-bacterial performance. The developed nanocomposite found effective against the biofilms of *S. aureus*. Magnetically-separable M-HNTs-ZnO gave significant anti-bacterial performance against *E. coli*, *S. aureus* and MRSA in repeated cycles. This marks the importance of M-HNTs-ZnO in water treatments. The coupling of potent anti-bacterial and magnetically-operable properties in M-HNTs-ZnO can be applied in the clinical treatment of pathogenic infections as well as for water treatment to remove/kill pathogenic bacteria's.

CRediT authorship contribution statement

Seung-Cheol Jee: Conceptualization, Methodology, Software, Writing - original draft. **Min Kim:** Methodology, Conceptualization. **Surendra K. Shinde:** Methodology. **Gajanan S. Ghodake:** Methodology. **Jung-Suk Sung:** Writing - review & editing. **Avinash A. Kadam:** Writing - review & editing, Supervision.

Declaration of Competing Interest

The authors declare that they have no known competing financial interests or personal relationships that could have appeared to influence the work reported in this paper.

Acknowledgment

This work was supported by the National Research Foundation of Korea (NRF) grant funded by the Korea government (MSIT) (NRF-2019R1G1A1009363). This work was also supported by a Grant (14162NRFS072) from the National Research Foundation (NRF, Korea, 2019). We would like to thank Dr. Park at the Korea Basic Science Institute Western Seoul Center for acquiring the SEM measurement.

Appendix A. Supplementary material

Supplementary data to this article can be found online at https://doi.org/10.1016/j.apsusc.2020.145358.

References

[1] A. Hibbitts, C. O'Leary, Emerging nanomedicine therapies to counter the rise of Methicillin-resistant Staphylococcus aureus, Materials (Basel). 11 (2018) 1–33, https://doi.org/10.3390/ma11020321.
[2] A. Gupta, S. Mumtaz, C.H. Li, I. Hussain, V.M. Rotello, Combatting antibiotic-resistant bacteria using nanomaterials, Chem. Soc. Rev. 48 (2019) 415–427, https://doi.org/10.1039/c7cs00748e.
[3] S. Satish, M. Tharmavaram, D. Rawtani, Halloysite nanotubes as a nature's boon for biomedical applications, 184954351986362, Nanobiomedicine. 6 (2019), https://doi.org/10.1177/1849543519863625.
[4] Y.J. Lee, S.C. Lee, S.C. Jee, J.S. Sung, A.A. Kadam, Surface functionalization of halloysite nanotubes with supermagnetic iron oxide, chitosan and 2-D calcium-phosphate nanoflakes for synergistic osteoconduction enhancement of human adipose tissue-derived mesenchymal stem cells, Coll. Surf. B Biointerf. 173 (2019) 18–26, https://doi.org/10.1016/j.colsurfb.2018.09.045.
[5] S. Jana, A.V. Kondakova, S.N. Shevchenko, E.V. Sheval, K.A. Gonchar, V.Y. Timoshenko, A.N. Vasiliev, Halloysite nanotubes with immobilized silver

nanoparticles for anti-bacterial application, Coll. Surf. B Biointerf. 151 (2017) 249–254, https://doi.org/10.1016/j.colsurfb.2016.12.017.
[6] Z. Shu, Y. Zhang, Q. Yang, H. Yang, Halloysite nanotubes supported Ag and ZnO Nanoparticles with synergistically enhanced antibacterial activity, Nanoscale Res. Lett. 12 (2017), https://doi.org/10.1186/s11671-017-1859-5.
[7] A.A. Kadam, J. Jang, D.S. Lee, Supermagnetically tuned halloysite nanotubes functionalized with aminosilane for covalent laccase immobilization, ACS Appl. Mater. Interf. 9 (2017) 15492–15501, https://doi.org/10.1021/acsami.7b02531.
[8] A.A. Kadam, J. Jang, S.C. Jee, J.S. Sung, D.S. Lee, Chitosan-functionalized supermagnetic halloysite nanotubes for covalent laccase immobilization, Carbohydr. Polym. 194 (2018) 208–216, https://doi.org/10.1016/j.carbpol.2018.04.046.
[9] P. Pasbakhsh, G.J. Churchman, J.L. Keeling, Characterisation of properties of various halloysites relevant to their use as nanotubes and microfibre fillers, Appl. Clay Sci. 74 (2013) 47–57, https://doi.org/10.1016/j.clay.2012.06.014.
[10] R.D. White, D.V. Bavykin, F.C. Walsh, The stability of halloysite nanotubes in acidic and alkaline aqueous suspensions, Nanotechnology 23 (2012), https://doi.org/10.1088/0957-4484/23/6/065705.
[11] V. Akbari, F. Najafi, H. Vahabi, M. Jouyandeh, M. Badawi, S. Morisset, M.R. Ganjali, M.R. Saeb, Surface chemistry of halloysite nanotubes controls the curability of low filled epoxy nanocomposites, Prog. Org. Coatings. 135 (2019) 555–564, https://doi.org/10.1016/j.porgcoat.2019.06.009.
[12] M. Tharmavaram, G. Pandey, D. Rawtani, Surface modified halloysite nanotubes: a flexible interface for biological, environmental and catalytic applications, Adv. Coll. Interf. Sci. 261 (2018) 82–101, https://doi.org/10.1016/j.cis.2018.09.001.
[13] S. Satish, M. Tharmavaram, D. Rawtani, Halloysite nanotubes as a nature's boon for biomedical applications, Nanobiomedicine. 6 (2019) 1–16, https://doi.org/10.1177/1849543519863625.
[14] G.I. Fakhrullina, F.S. Akhatova, Y.M. Lvov, R.F. Fakhrullin, Toxicity of halloysite clay nanotubes in vivo: a Caenorhabditis elegans study, Environ. Sci. Nano. 2 (2015) 54–59, https://doi.org/10.1039/c4en00135d.
[15] Z. Long, Y.P. Wu, H.Y. Gao, J. Zhang, X. Ou, R.R. He, M. Liu, In vitro and in vivo toxicity evaluation of halloysite nanotubes, J. Mater. Chem. B. 6 (2018) 7204–7216, https://doi.org/10.1039/c8tb01382a.
[16] A.C. Santos, I. Pereira, S. Reis, F. Veiga, M. Saleh, Y. Lvov, Biomedical potential of clay nanotube formulations and their toxicity assessment, Expert Opin. Drug Deliv. 16 (2019) 1169–1182, https://doi.org/10.1080/17425247.2019.1665020.
[17] R. Abhinayaa, G. Jeevitha, D. Mangalaraj, N. Ponpandian, K. Vidhya, J. Angayarkanni, Cytotoxic consequences of Halloysite nanotube/iron oxide nanocomposite and iron oxide nanoparticles upon interaction with bacterial, non-cancerous and cancerous cells, Coll. Surf. B Biointerf. 169 (2018) 395–403, https://doi.org/10.1016/j.colsurfb.2018.05.040.
[18] J.C. Monteiro, I.M. Garcia, V.C.B. Leitune, F. Visioli, G. de Souza Balbinot, S.M.W. Samuel, I. Makeeva, F.M. Collares, S. Sauro, Halloysite nanotubes loaded with alkyl trimethyl ammonium bromide as antibacterial agent for root canal sealers, Dent. Mater. 35 (2019) 789–796, https://doi.org/10.1016/j.dental.2019.02.018.
[19] S. Hendessi, E.B. Sevinis, S. Unal, F.C. Cebeci, Y.Z. Menceloglu, H. Unal, Antibacterial sustained-release coatings from halloysite nanotubes/waterborne polyurethanes, Prog. Org. Coatings. 101 (2016) 253–261, https://doi.org/10.1016/j.porgcoat.2016.09.005.
[20] G. Biddeci, G. Cavallaro, F. Di Blasi, G. Lazzara, M. Massaro, S. Milioto, F. Parisi, S. Riela, G. Spinelli, Halloysite nanotubes loaded with peppermint essential oil as filler for functional biopolymer film, Carbohydr. Polym. 152 (2016) 548–557, https://doi.org/10.1016/j.carbpol.2016.07.041.
[21] M.H. Lee, H.S. Seo, H.J. Park, Thyme oil encapsulated in halloysite nanotubes for antimicrobial packaging system, J. Food Sci. 82 (2017) 922–932, https://doi.org/10.1111/1750-3841.13675.
[22] L. Yu, Y. Zhang, B. Zhang, J. Liu, Enhanced antibacterial activity of silver nanoparticles/halloysite nanotubes/graphene nanocomposites with sandwich-like structure, Sci. Rep. 4 (2014) 1–5, https://doi.org/10.1038/srep04551.
[23] Q. Pan, N. Li, Y. Hong, H. Tang, Z. Zheng, S. Weng, Y. Zheng, L. Huang, Halloysite clay nanotubes as effective nanocarriers for the adsorption and loading of vancomycin for sustained release, RSC Adv. 7 (2017) 21352–21359, https://doi.org/10.1039/c7ra00376e.
[24] A. Stavitskaya, S. Batasheva, V. Vinokurov, G. Fakhrullina, V. Sangarov, Y. Lvov, R. Fakhrullin, Antimicrobial applications of clay nanotube-based composites, Nanomaterials. 9 (2019) 708, https://doi.org/10.3390/nano9050708.
[25] L. Arias, J. Pessan, A. Vieira, T. Lima, A. Delbem, D. Monteiro, Iron oxide nanoparticles for biomedical applications: a perspective on synthesis, Drugs Antimicrob. Activity Toxicity Antibiot. 7 (2018) 46, https://doi.org/10.3390/antibiotics7020046.
[26] B. Lallo da Silva, B.L. Caetano, B.G. Chiari-Andréo, R.C.L.R. Pietro, L.A. Chiavacci, Increased antibacterial activity of ZnO nanoparticles: Influence of size and surface modification, Coll. Surf. B Biointerf. 177 (2019) 440–447, https://doi.org/10.1016/J.COLSURFB.2019.02.013.
[27] A. Sirelkhatim, S. Mahmud, A. Seeni, N.H.M. Kaus, L.C. Ann, S.K.M. Bakhori, H. Hasan, D. Mohamad, Review on zinc oxide nanoparticles: Antibacterial activity and toxicity mechanism, Nano-Micro Lett. 7 (2015) 219–242, https://doi.org/10.1007/s40820-015-0040-x.
[28] J. Li, M. Zhou, Z. Ye, H. Wang, C. Ma, P. Huo, Y. Yan, Enhanced photocatalytic activity of g-C3N4-ZnO/HNT composite heterostructure photocatalysts for degradation of tetracycline under visible light irradiation, RSC Adv. 5 (2015) 91177–91189, https://doi.org/10.1039/c5ra17360d.
[29] A. Baltakesmez, M. Biber, S. Tüzemen, Inverted planar perovskite solar cells based on Al doped ZnO substrate, J. Radiat. Res. Appl. Sci. 11 (2018) 124–129, https://doi.org/10.1016/j.jrras.2017.11.002.
[30] H. Wang, S. Cao, B. Yang, H. Li, M. Wang, X. Hu, K. Sun, Z. Zang, NH 4 Cl modified ZnO for high-performance CsPbIBr 2 perovskite solar cells via low temperature process, Sol. RRL. 1900363 (2019) 1–8, https://doi.org/10.1002/solr.201900363.
[31] K. Zhu, Y. Duan, F. Wang, P. Gao, H. Jia, C. Ma, C. Wang, Silane-modified halloysite/Fe3O4 nanocomposites: Simultaneous removal of Cr(VI) and Sb(V) and positive effects of Cr(VI) on Sb(V) adsorption, Chem. Eng. J. 311 (2017) 236–246, https://doi.org/10.1016/j.cej.2016.11.101.
[32] H. Peng, X. Liu, W. Tang, R. Ma, Facile synthesis and characterization of ZnO nanoparticles grown on halloysite nanotubes for enhanced photocatalytic properties, Sci. Rep. 7 (2017) 1–10, https://doi.org/10.1038/s41598-017-02501-w.
[33] K. Lim, W.S. Chow, S.Y. Pung, Enhancement of thermal stability and UV resistance of halloysite nanotubes using zinc oxide functionalization via a solvent-free approach, Int. J. Miner. Metall. Mater. 26 (2019) 787–795, https://doi.org/10.1007/s12613-019-1781-1.
[34] K. Min, S.C. Jee, J.S. Sung, A.A. Kadam, Anti-proliferative applications of laccase immobilized on super-magnetic chitosan-functionalized halloysite nanotubes, Int. J. Biol. Macromol. (2018), https://doi.org/10.1016/j.ijbiomac.2018.06.074.
[35] N.Y. Choi, B.R. Kim, Y.M. Bae, S.Y. Lee, Biofilm formation, attachment, and cell hydrophobicity of foodborne pathogens under varied environmental conditions, J. Korean Soc. Appl. Biol. Chem. 56 (2013) 207–220, https://doi.org/10.1007/s13765-012-3253-4.
[36] P. Yuan, P.D. Southon, Z. Liu, M.E.R. Green, J.M. Hook, S.J. Antill, C.J. Kepert, Functionalization of halloysite clay nanotubes by grafting with γ-aminopropyltriethoxysilane, J. Phys. Chem. C. 112 (2008) 15742–15751, https://doi.org/10.1021/jp805657t.
[37] C.R. Martinez, P. Joshi, J.L. Vera, J.E. Ramirez-Vick, O. Perales, S.P. Singh, Cytotoxic studies of PEG functionalized ZnO nanoparticles on MCF-7 cancer cells, Tech. Proc. 2011 NSTI Nanotechnol. Conf. Expo, NSTI-Nanotech 2011, (2011).
[38] D.H.K. Reddy, S.M. Lee, Application of magnetic chitosan composites for the removal of toxic metal and dyes from aqueous solutions, Adv. Coll. Interf. Sci. 201–202 (2013) 68–93, https://doi.org/10.1016/j.cis.2013.10.002.
[39] R. Madhuvilakku, S. Alagar, R. Mariappan, S. Piraman, Green one-pot synthesis of flowers-like Fe3O4/rGO hybrid nanocomposites for effective electrochemical detection of riboflavin and low-cost supercapacitor applications, Sens. Actuat. B Chem. 253 (2017) 879–892, https://doi.org/10.1016/j.snb.2017.06.126.
[40] M. Navaneethan, G.K. Mani, S. Ponnusamy, K. Tsuchiya, C. Muthamizhchelvan, S. Kawasaki, Y. Hayakawa, Influence of Al doping on the structural, morphological, optical, and gas sensing properties of ZnO nanorods, J. Alloys Compd. 698 (2017) 555–564, https://doi.org/10.1016/j.jallcom.2016.12.187.
[41] A.A. Taylor, G.M. Aron, G.W. Beall, N. Dhamasiri, Y. Zhang, R.J.C. McLean, Carbon and clay nanoparticles induce minimal stress responses in gram negative bacteria and eukaryotic fish cells, Environ. Toxicol. 29 (2012) 961–968, https://doi.org/10.1002/tox.21824.
[42] A.K. Gupta, M. Gupta, Synthesis and surface engineering of iron oxide nanoparticles for biomedical applications, Biomaterials 26 (2005) 3995–4021, https://doi.org/10.1016/j.biomaterials.2004.10.012.
[43] H. Dong, J. Huang, R.R. Koepsel, P. Ye, A.J. Russell, K. Matyjaszewski, Recyclable antibacterial magnetic nanoparticles grafted with quaternized poly(2-(dimethylamino)ethyl methacrylate) brushes, Biomacromolecules 12 (2011) 1305–1311, https://doi.org/10.1021/bm200031v.
[44] L. Ghezzi, A. Spepi, M. Agnolucci, C. Cristani, M. Giovannetti, M.R. Tiné, C. Duce, Kinetics of release and antibacterial activity of salicylic acid loaded into halloysite nanotubes, Appl. Clay Sci. 160 (2018) 88–94, https://doi.org/10.1016/j.clay.2017.11.041.
[45] L. Duan, Q. Zhao, J. Liu, Y. Zhang, Antibacterial behavior of halloysite nanotubes decorated with copper nanoparticles in a novel mixed matrix membrane for water purification, Environ. Sci. Water Res. Technol. 1 (2015) 874–881, https://doi.org/10.1039/c5ew00140d.
[46] S.S. Suner, M. Sahiner, A. Akcali, N. Sahiner, Functionalization of halloysite nanotubes with polyethyleneimine and various ionic liquid forms with antimicrobial activity, J. Appl. Polym. Sci. 137 (2020) 1–10, https://doi.org/10.1002/app.48352.
[47] S. Saadat, G. Pandey, M. Tharmavaram, V. Braganza, D. Rawtani, Nano-interfacial decoration of halloysite nanotubes for the development of antimicrobial nanocomposites, Adv. Coll. Interf. Sci. 102063 (2019), https://doi.org/10.1016/j.cis.2019.102063.
[48] Y. Zhang, Y. Chen, H. Zhang, B. Zhang, J. Liu, Potent antibacterial activity of a novel silver nanoparticle-halloysite nanotube nanocomposite powder, J. Inorg. Biochem. 118 (2013) 59–64, https://doi.org/10.1016/j.jinorgbio.2012.07.025.
[49] Z. Shu, Y. Zhang, J. Ouyang, H. Yang, Characterization and synergetic antibacterial properties of ZnO and CeO2 supported by halloysite, Appl. Surf. Sci. 420 (2017) 833–838, https://doi.org/10.1016/j.apsusc.2017.05.219.
[50] S. Chakraborti, A.K. Mandal, S. Sarwar, P. Singh, R. Chakraborty, P. Chakrabarti, Bactericidal effect of polyethyleneimine capped ZnO nanoparticles on multiple antibiotic resistant bacteria harboring genes of high-pathogenicity island, Coll. Surf. B Biointerf. 121 (2014) 44–53, https://doi.org/10.1016/j.colsurfb.2014.03.044.
[51] A. Hassoun, P.K. Linden, B. Friedman, Incidence, prevalence, and management of MRSA bacteremia across patient populations-a review of recent developments in MRSA management and treatment, Crit. Care. 21 (2017) 211, https://doi.org/10.1186/s13054-017-1801-3.
[52] G. Rajivgandhi, M. Maruthupandy, T. Muneeswaran, M. Anand, N. Manoharan, Antibiofilm activity of zinc oxide nanosheets (ZnO NSs) using Nocardiopsis sp. GRG1 (KT235640) against MDR strains of gram negative Proteus mirabilis and Escherichia coli, Process Biochem. 67 (2018) 8–18, https://doi.org/10.1016/J.PROCBIO.2018.01.015.
[53] G. Sahni, P. Gopinath, P. Jeevanandam, A novel thermal decomposition approach to synthesize hydroxyapatite-silver nanocomposites and their antibacterial action

against GFP-expressing antibiotic resistant E. coli, Coll. Surf. B Biointerf. 103 (2013) 441–447, https://doi.org/10.1016/j.colsurfb.2012.10.050.
[54] A. Panáček, M. Smékalová, R. Večeřová, K. Bogdanová, M. Röderová, M. Kolář, M. Kilianová, Š. Hradilová, J.P. Froning, M. Havrdová, R. Prucek, R. Zbořil, L. Kvítek, Silver nanoparticles strongly enhance and restore bactericidal activity of inactive antibiotics against multiresistant Enterobacteriaceae, Coll. Surf. B Biointerf. 142 (2016) 392–399, https://doi.org/10.1016/j.colsurfb.2016.03.007.
[55] I. Matai, A. Sachdev, P. Dubey, S. Uday Kumar, B. Bhushan, P. Gopinath, Antibacterial activity and mechanism of Ag-ZnO nanocomposite on S. aureus and GFP-expressing antibiotic resistant E. coli, Coll. Surf. B Biointerf. 115 (2014) 359–367, https://doi.org/10.1016/j.colsurfb.2013.12.005.
[56] K. Niemirowicz, E. Piktel, A.Z. Wilczewska, K.H. Markiewicz, B. Durnas, M. Watek, I. Puszkarz, M. Wróblewska, W. Niklinska, P.B. Savage, R. Bucki, Core-shell magnetic nanoparticles display synergistic antibacterial effects against and when combined with cathelicidin LL-37 or selected ceragenins, Int. J. Nanomed. 11 (2016) 5443–5455, https://doi.org/10.2147/IJN.S113706.
[57] P.V. Baptista, M.P. McCusker, A. Carvalho, D.A. Ferreira, N.M. Mohan, M. Martins, A.R. Fernandes, Nano-strategies to fight multidrug resistant bacteria-"A Battle of the Titans", Front. Microbiol. 9 (2018) 1–26, https://doi.org/10.3389/fmicb.2018.01441.
[58] E.H. Abdulkareem, K. Memarzadeh, R.P. Allaker, J. Huang, J. Pratten, D. Spratt, Anti-biofilm activity of zinc oxide and hydroxyapatite nanoparticles as dental implant coating materials, J. Dent. 43 (2015) 1462–1469, https://doi.org/10.1016/J.JDENT.2015.10.010.
[59] P.Y. Furlan, A.J. Fisher, A.Y. Furlan, M.E. Melcer, D.W. Shinn, J.B. Warren, Magnetically recoverable and reusable antimicrobial nanocomposite based on activated carbon, magnetite nanoparticles, and silver nanoparticles for water disinfection, Inventions 2 (2017), https://doi.org/10.3390/inventions2020010.
[60] S.W. Krasner, H.S. Weinberg, S.D. Richardson, S.J. Pastor, R. Chinn, M.J. Sclimenti, G.D. Onstad, A.D. Thruston, Occurrence of a new generation of disinfection byproducts, Environ. Sci. Technol. 40 (2006) 7175–7185, https://doi.org/10.1021/es060353j.
[61] R.G. Suthar, B. Gao, Nanotechnology for drinking water purification, Water Purif. (2017) 75–118, https://doi.org/10.1016/B978-0-12-804300-4.00003-4.
[62] C. Martinez-Boubeta, K. Simeonidis, Magnetic nanoparticles for water purification, Nanoscale Mater Water Purif. (2019) 521–552, https://doi.org/10.1016/B978-0-12-813926-4.00026-4.
[63] E.I. Unuabonah, C.G. Ugwuja, M.O. Omorogie, A. Adewuyi, N.A. Oladoja, Clays for efficient disinfection of bacteria in water, Appl. Clay Sci. 151 (2018) 211–223, https://doi.org/10.1016/j.clay.2017.10.005.